Lipid composition of the membrane governs the oligomeric organization of VDAC1

Elodie Lafargue[1#], Jean-Pierre Duneau[2#], Nicolas Buzhinsky[1], Pamela Ornelas[3], Alexandre Ortega[1], Varun Ravishankar[2], James Sturgis[2], Ignacio Casuso[1]*, Lucie Bergdoll[2]*

[1]U1325 DyNaMo INSERM, Aix-Marseille Université, Turing Centre for Living System, Marseille, France, [2]Laboratoire d'Ingénierie des Systèmes Macromoléculaires, CNRS - Aix Marseille Université, 31 Chemin Joseph Aiguier, Marseille, [3]Department of Structural Biology, Max- Planck- Institute of Biophysics, Frankfurt 60438, Germany
* : corresponding authors
#: these authors contributed equally to this work

Mitochondrial physiology is intricately linked to the oligomerization of voltage-dependent anion channels (VDAC), acting as gatekeepers to mitochondria. However, the molecular determinants of VDAC oligomerization remain poorly understood. Here, we used atomic force microscopy to investigate the effects of three lipids of the Mitochondrial Outer Membrane (MOM) on VDAC assemblies. We observed that VDAC forms lipid-sensitive clusters, termed honeycombs, and their compaction is regulated by cholesterol. Molecular dynamics simulations revealed VDAC's affinity for cholesterol and phosphatidylethanolamine, both of which affect the formation of these honeycombs. Although we identified honeycomb-like assemblies akin to those in the native MOM, deviations from the physiological lipid composition resulted in varying degrees of disruption of these native-like structures. This emphasizes the profound impact of the lipid environment on VDAC organization. These findings underscore the physiological significance of lipid heterogeneity and changes within biological membranes arising from membrane contacts or pathologies in modulating VDAC behavior.

Introduction

The Voltage-Dependent Anion channel (VDAC) is by far the most abundant protein (>50% molar)[1,2] in the Mitochondrial Outer Membrane (MOM), playing crucial roles in many cellular functions. In addition to facilitating the passage of ions and metabolites like ATP and ADP across the membrane, VDAC is involved in numerous mitochondrial regulatory processes such as apoptosis[3–5], calcium homeostasis[6,7], mtDNA release[8] and lipid scrambling[9]. VDAC act as gatekeepers to the mitochondria, anchoring different cytosolic proteins that interact with the organelle and are suspected to have up to 100 partners[10], including pro-apoptotic proteins Bax and Bak[4,11], tubulin[12,13], synuclein[14,15], TSPO[16] and hexokinase[17].

VDAC's ability to engage in multiple and sometimes opposing signaling pathways (e.g., anti- and pro-apoptotic) requires precise regulation of the interactions of VDAC with its partners. In mammals, VDAC has three isoforms, each partnering with distinct proteins involved in different pathways[4,15]. The oligomeric organization of VDAC in the membrane adds another level of regulation, influencing its functional adaptability in various cellular contexts. *In vitro*, VDAC can adopt diverse oligomeric states, as evidenced by multiple techniques[18–22], which could serve as platforms to recruit specific partners.

VDAC is embedded in the lipid bilayer, with protein-lipid interactions playing a major role in its function[23–25]. Lipid composition can regulate VDAC interactions with several partner proteins[14,26], and cholesterol and neurosteroid-binding sites have been identified on VDAC1[27–29]. VDAC tends to oligomerize in lipid environments[19,21,30], with some lipids favoring oligomerization[19].

Investigating VDAC assembly at the single-molecule level in lipids is challenging, but Atomic Force Microscopy (AFM) is well-suited for assessing protein organization in membranes. VDAC, a 19-strand β-barrel, has a specific AFM signature of a 4.5-nm pore (Fig. 1d). In 2007, two independent AFM studies on MOM derived from yeast[1] and potato tuber[2] described multiple assemblies of VDAC in native membranes, with a predominance of large assemblies. While both studies are pivotal to understanding VDAC behavior in the membrane, additional proteins beyond VDAC are present in the native

membrane, and the specific lipid composition of the membrane was not controlled. This is significant because the lipid content can vary under different physiological conditions or diseases (cancer, apoptosis and neurodegeneration)[31–33]. Besides, lipid distribution in biological membranes is heterogeneous and dynamic and can vary rapidly at contact sites (with the mitochondrial inner membrane or the endoplasmic reticulum (ER) membrane). Given the dynamic nature of membrane composition under physiological conditions and in pathological states, elucidating the influence of lipid composition on VDAC organization is of utmost importance.

In this study, we use a combination of AFM and Molecular Dynamics (MD) simulations in a controlled lipid environment to explore the influence of principal MOM lipids, phosphatidylcholine (PC), phosphatidylethanolamine (PE) (the main species being POPC and POPE), and cholesterol on VDAC1 organization. We revealed that VDAC1 precisely tunes its surrounding lipids, leading to the formation of specific assemblies controlled by membrane lipid composition. This sensitivity of VDAC assembly to lipids enables flexible and rapid reorganization of VDAC in the MOM in response to changing conditions, serving as a regulatory mechanism for interaction of VDAC with its different partners, thus tuning its function.

Results

To allow for the study of VDAC assembly in an environment close to the MOM, while allowing the control of all parameters, we used a system composed of purified VDAC1 reconstituted in controlled lipid environments containing various mixtures of the three main lipids of the MOM: two phospholipids (POPC and POPE) and cholesterol at various ratios. VDAC-containing liposomes were then adsorbed onto a mica surface and imaged by AFM (Fig. 1). Several lipid to protein ratios (LPR) were tested, and LPR 3:1 (w:w, corresponding to a 40:1 molar ratio) was selected as it led to a surface density similar to that observed in native MOM[1,2]. All experiments were performed in triplicate at temperatures above 33°C to avoid lipidic phase separation and membrane partitioning (SFig. 1).

VDAC adopts different organizations in different lipid compositions

Using POPC, POPE, and cholesterol, we explored various lipid ratios and compositions for VDAC1 reconstitution. SFig. 2 is a gallery of images showing drastically different shapes, compaction, and density of VDAC proteins, visible in lighter colors on a homogenous dark-brown lipid background. These observations, reproducible across experiments, highlight the diverse organizational patterns triggered by changes in lipid composition, and hence the crucial role of lipids in regulating VDAC assemblies. In particular, dense assemblies of tightly packed clusters (SFig. 2f, g), in contrast to the more loosely arranged configurations (SFig. 2b,d), highlighting the variability in assembly due to lipid types and their ratios. In subsequent sections, we focus on these structures, their specific configurations under different lipid conditions, and their impact on VDAC assembly.

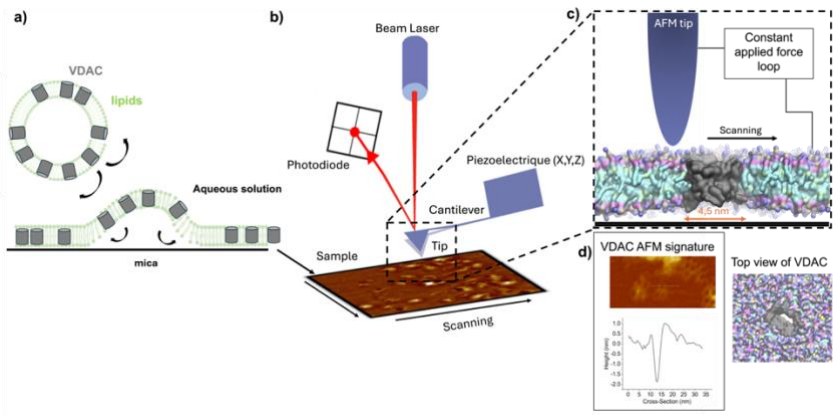

Fig. 1: General schematic of AFM experiment. a VDAC1 reconstituted in vesicles of different lipid compositions was adsorbed on a mica surface. **b** Diagram of AFM principle. The tip, positioned on a lever, scans the sample. A laser beam is used to detect the bending of the lever during the scanning. The laser is reflected by the lever on the photodiode. **c** Zoom from b on the interaction between the tip and the sample surface. The sample-to-tip distance is controlled by the feedback loop to keep the force applied to the sample constant. **d** AFM signature of a VDAC pore and its profile showing a diameter similar to the expected size of 4.5nm

VDAC forms protein-lipid clusters : honeycombs

We initially reconstituted VDAC in two primary lipids found in the mitochondrial outer membrane (MOM), POPC and POPE, in ratios closely resembling those of the native MOM (65:35 w:w, Table S1 describes the lipid ratios in the MOM under healthy conditions[34]). We observed the emergence of very stable (over several minutes) and densely packed assemblies composed of VDAC molecules and lipids, which we term "honeycombs," due to their resemblance to the hexagonal structure made by bees (Fig. 2a).

Appearing organized at first glance, a more detailed analysis based on a computerized model derived from the locations of the proteins identified by AFM (Fig. 2b, see methods) reveals intrinsic disorder within these assemblies, arranged in a non-crystalline manner, also termed glass-like organization. The term "glass-like" characterizes both disorganized crowding and amorphous assembly[35]. Our computerized model of the VDAC honeycomb, generated based on the AFM position of the VDAC molecules and MD simulations (see Methods and below), reveals both protein-protein and protein-lipid interactions mediated by lipids. This underscores the critical role of lipids in honeycomb formation. The outermost lipid shell, depicted in yellow in Fig. 2b, represents lipids directly interacting with the protein (approximately 20 per leaflet; SFig. 3). Notably, these honeycombs are very stable as the lipids act as "mortar" keeping the proteins in close proximity to each other, but not always in direct contact. Interestingly, the honeycomb structures (formed within membranes containing only POPC and POPE) closely resembled the organizational patterns observed in a subset of the population within the native MOM of potato tuber[2] and yeast[1] previously visualized by AFM. Additionally, negative staining imaging of outer membrane vesicles derived from *Neurospora crassa* revealed a similar pattern of VDAC organization within the native membrane (Fig. 2c,d). Collectively, these findings point to the physiological relevance of honeycomb organization.

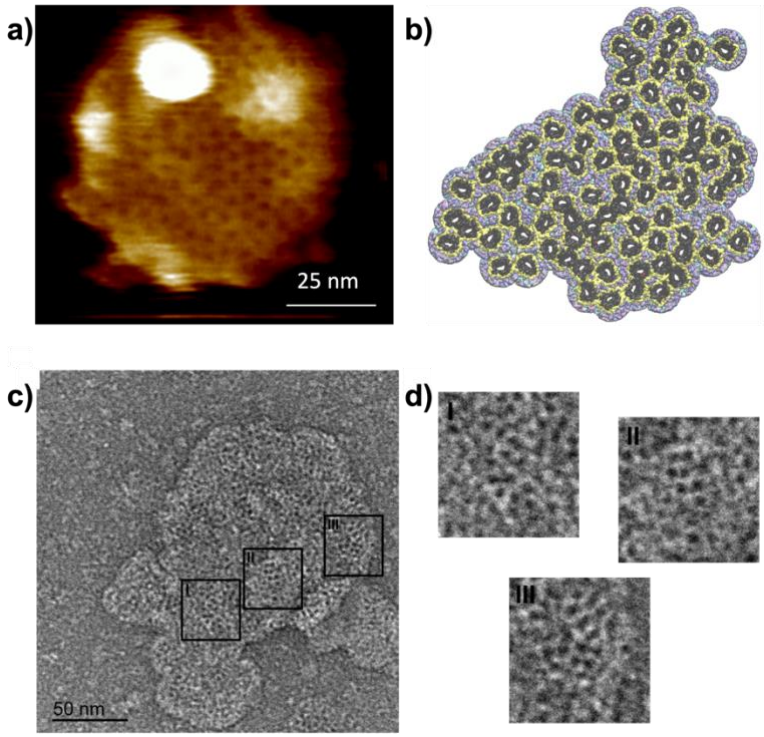

Figure 2: VDAC forms honeycombs. a AFM topography of VDAC1 in the POPC/POPE (65/35 w:w) membranes. All AFM measurements were performed at least in triplicate. **b** Computer model derived from AFM image in **a** (see methods). VDAC is depicted as a dark solid surface, with the first lipid shell in yellow, and the other interstitial lipids in an atom color-coded representation. **c** Electron micrograph of outer membrane vesicles from *Neurospora crassa* mitochondria stained with uranyl formate at 68,000 x magnification, showing VDAC honeycomb-like assemblies. **d** the higher resolution of the three different areas from **c**, shows that individual VDAC pores assemble as honeycombs.

The Honeycombs are parallel organizations of VDAC1

VDAC1 adopts a 2_1 screw axes symmetry in DMPC bilayers[36]; that is, along one crystallographic axis, the protein alternates between the right-side up and upside-down orientations. Such an antiparallel arrangement is frequently observed with membrane proteins and mainly arises from two factors: inherent asymmetry of the protein and charge asymmetry of the membrane bilayer. Hence, forming an anti-parallel organization with alternating orientations improves protein-protein interactions.

However, such an orientation cannot be physiological; therefore it is crucial to establish the orientation of VDAC in the honeycombs.

We developed a new method named "nanobead-mediated orientation determination," where a gold nanoparticle of 5 nm, functionalized with a Ni-NTA group, is attached to the 6His-tag of VDAC1 facing the intermembrane space (IMS) side of the protein (Fig. 3a). Using this method, we showed that VDAC is associated into parallel organization within the honeycombs (Fig. 3b,c), forming domains of parallel proteins that extend for tens of nanometers. We were able to image both orientations, the IMS-facing and the cytoplasm-facing clusters (SFig. 4). During reconstitution, VDAC forms parallel honeycomb structures within vesicles, exhibiting both possible orientations (cytoplasmic or IMS side), subsequently adhering to mica for AFM imaging and revealing dual orientations. This, coupled with the presence of honeycombs in native MOMs, confirms the physiological relevance of this organization.

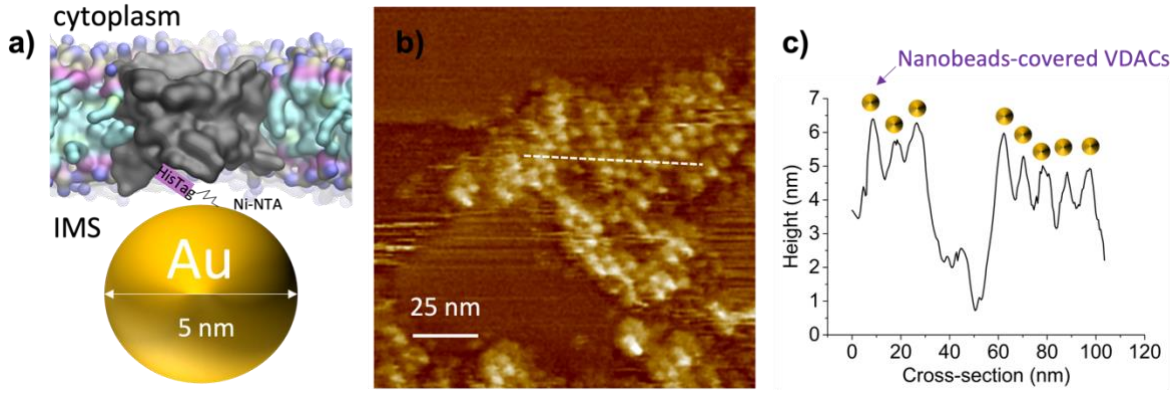

Fig. 3: VDAC forms parallel clusters. **a** Schematic representation of a new methods for orientation determination in AFM using gold nanoparticles coupled with Ni-NTA. The nanoparticles bind to the IMS-facing 6histag of VDAC and change the AFM profile. The distance between the bead and the His-tag is around 1.5 nm. **b** AFM imaging of honeycomb in presence of gold nanoparticles reveals a parallel orientation of the molecules. **c** Height profile from b) reveals peaks of the nanobead-covered VDAC, replacing the previous holes from the VDAC pores. Additional images are available on SFig. 4.

Cholesterol modulates honeycomb assembly

Cholesterol is a major component of MOMs (between 5% and 10% w:w; see Table S1) and is known to interact directly with VDAC at several identified binding sites[34,37]. The risk when working with cholesterol is to observe lipid phase perturbations owing to its capacity to induce liquid ordered (Lo) phases, distinct from the gel phase (Lβ) and the liquid disordered phase. However, these phase appearances are more noticeable in mixtures with saturated lipids or those with different melting temperatures, unlike our study, which used a phospholipid mixture with a uniform acyl chain. NMR studies demonstrate cholesterol's high compatibility with such lipids, requiring substantial amounts (approximately 17% w:w) to significantly alter acyl chain ordering[38]. In our experiments above 33°C, cholesterol remained well mixed with phospholipids without forming phase separations, as tested beforehand in membranes lacking VDAC (SFig. 1).

Although honeycombs can form in POPC/POPE membranes without cholesterol, we investigated the effect of varying cholesterol concentrations (from 2% to 10%) on VDAC organization (Fig. 4). Even at modest cholesterol levels, we observed significant alterations in the assemblies, leading to a wide range of behaviors and oligomeric formations, as depicted in Fig. 4.

Remarkably, the addition of only 2% cholesterol to the POPC/POPE lipid mixture that created honeycombs resulted in a dramatic transformation of the assemblies, as evidenced by AFM micrographs (Fig. 4a-d): most of the molecules were no longer in honeycombs but aligned in strands of a few molecules in width, where the membrane tends to bend. The assembly of the proteins is less compact and more dynamic, making the individual pores of VDAC scarcely visible by AFM, rendering most protein positions in the 2% cholesterol conditions appear loosely defined, despite the high resolution of the micrographs. To better visualize this behavior we changed the parameters for protein identification and used three set of conditions which are either more or less stringent that the software assisted

parameters. This resulted in the image depicted in Fig. 4d, where a core of 35 proteins (blue) are robustly associated with all three collections. The two less stringent procedures yielded 63 (yellow) and 82 (magenta) proteins, respectively. The superposition also illustrates the overall good alignment of the core proteins across the three distinct evaluations.

Even more remarkably, when the cholesterol content was increased to 5%, the organization of VDACs progressively returned to honeycomb organization, although with smaller and more linear honeycombs compared to those observed in the POPC/POPE membranes at 65/35 (Fig. 2a). Under these conditions, small protein patches of honeycomb structures resembling those imaged in 2007 on native MOM[2] began to appear. When the cholesterol content increased to 7.5%, the linearity of VDAC assembly decreased, resembling native MOM conditions more closely. VDAC assemblies maintained a honeycomb structure, with more patches observed, similar to those seen at 5% cholesterol and in native MOM conditions. The linearity factor decreased and the compaction and extension increased. This trend is confirmed and more pronounced in PC/PE/10%Chol bilayers (Fig. 4l-o), where extended (up to several μm) and compact honeycomb assemblies alternate with lipid areas. Within the honeycombs, small lipid patches were also observed: VDAC selected its ideal lipid-protein ratio, while leftover lipids accumulated in these patches. Overall, we conclude that although cholesterol is not essential for honeycombs formation, it significantly influences their assembly, particularly impacting their compaction and linearity.

Physiological lipid ratios are essential for a native VDAC organization

To further explore the impact of variable lipid ratios on VDAC organization we tested different lipid compositions. In natural MOM, the lipid ratio PC/PE/Chol is approximately 60/30/10, and as already shown, this produces the honeycomb structure of VDAC observed on natural MOM (Table S1). Thus, the PC/PE/Chol 2% condition, forming small filaments of aligned VDACs, was beyond the physiological range, which is probably why it was not previously observed in the native MOM. Omitting cholesterol resulted in filaments and irregular lipid barriers of VDAC for a 50/50 mixture of POPC/POPE (SFig. 6a) but allowed for honeycomb formation using close to natural ratio 65/35 (Fig. 2a). Omitting POPE even at cholesterol concentrations up to 10% failed to rescue honeycomb formation (SFig. 6b) indicating the necessity of POPE for such structures.

Analysis of VDAC organization reveals molecular interactions

To better understand the lipid-VDAC relationship, we used protein positions from AFM micrographs to construct molecular models (Fig. 2 and 4 and described in Methods), allowing to establish distance relationships between proteins using Radial Distribution Functions (describing pore-pore distance probability, SFig. 7) and explore the lipid environment influencing these distances. We categorized interactions based on radial distribution functions into direct protein-protein interactions, lipid-bridged interactions, and mixed lipid-protein bridged interactions (Fig. 5). This classification clarifies protein-lipid interplay in the membrane, highlighting increased compaction with higher cholesterol levels. SFig. 5 shows the models at higher magnification to better visualize lipid roles. Discrete peaks in the Radial Distribution Functions (SFig. 7) reveal a "rule of 6 Å," representing the average size of successive lipid shells in lipid-bridged protein separations. However, as the distance increased, the distinction between lipid-bridged and protein-bridged VDAC-to-VDAC distance diminished.

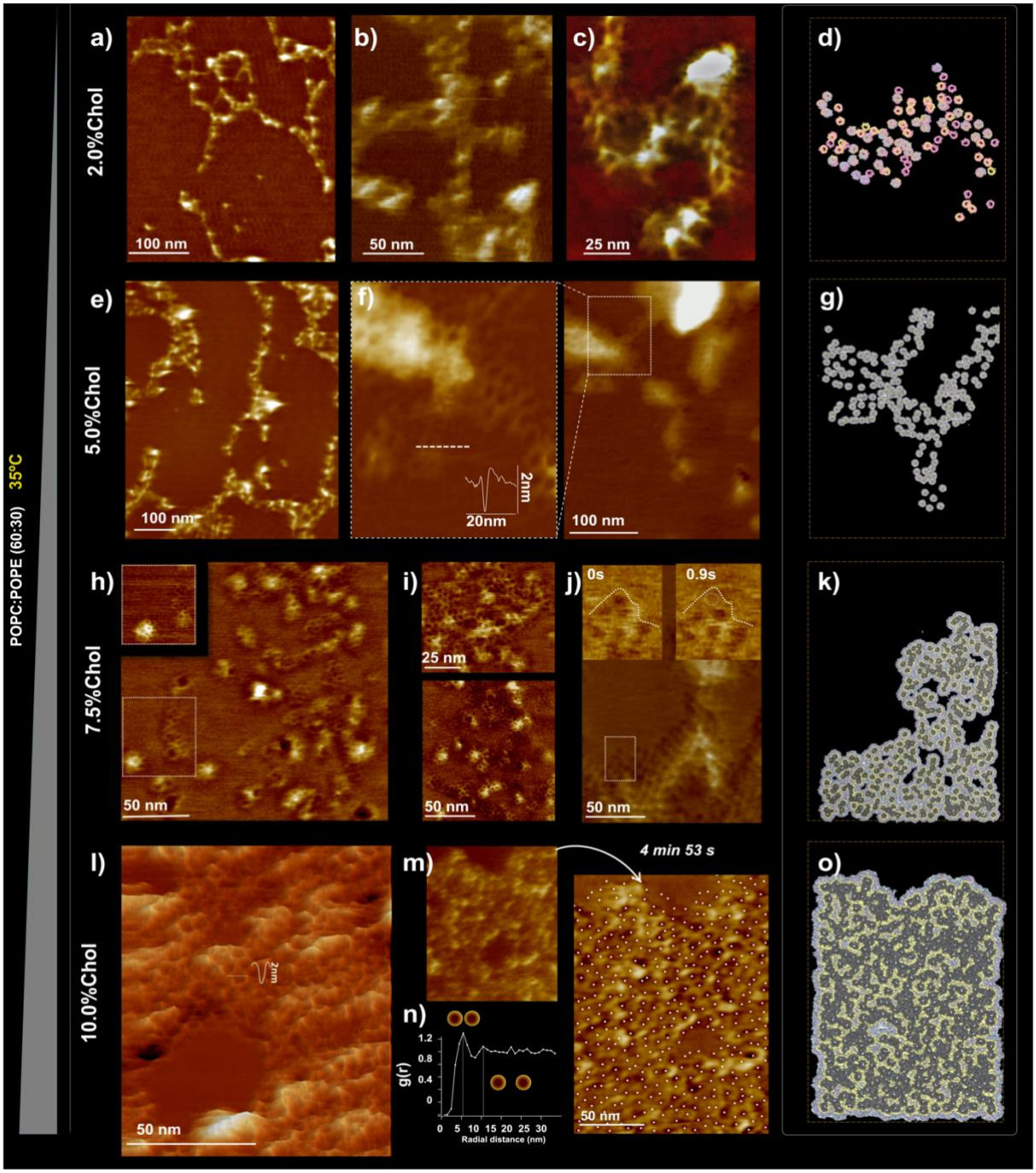

Fig. 4. Cholesterol controls the packing of VDAC honeycombs on POPC:POPE bilayers (60:30). AFM imaging at 33°C. The height of the false-color scale in all images was 11 nm. At 2.0% Chol **a**, **b**, and **c**, the assemblies were linear and curved the membrane. **e** At 5.0% cholesterol, the assembly was also linear, but significant honeycomb aggregations were observed. **f** Rows of VDAC are formed by one or a few pores in the transverse direction. **h** and **i** At 7.5% cholesterol, the honeycombs of VDAC were more prevalent. **j** Very rarely, an isolated pore moves to the border of the assembly, as shown in the inset. **l** At 10.0% cholesterol, the linearity of the VDAC arrangement was lost, and VDAC formed dense homogeneous assemblies with a rough topography. **m** The assemblies were stable as long as they were observed in all cholesterol conditions. **n** The inter-pore distance probability (radial distribution function) obtained from the positions of the pores in a dense assembly localized by cross-correlation showed that the most probable distance between VDACs is of 5.5 nm, and a second smaller peak shows at 10.5 nm. *Right panel*: Model of complexes. The development of a coarse-grained molecular model from the various assemblies **d** from **c**, **g** from zoom in **f**, **k** from **j**, and **o** from m allows us to accurately determine the context of protein-lipid interactions that support these distances. In **d**, only VDAC molecules are represented, with blue corresponding to the positions with higher confidence, yellow and magenta, with two lower degrees of confidence, respectively. In **g**, **k**, **o**, VDAC is depicted as a dark solid surface, with the first lipid shell in yellow

and the other interstitial lipids in an atom color-coded representation. The higher resolution of these models is shown in SFig. 5.

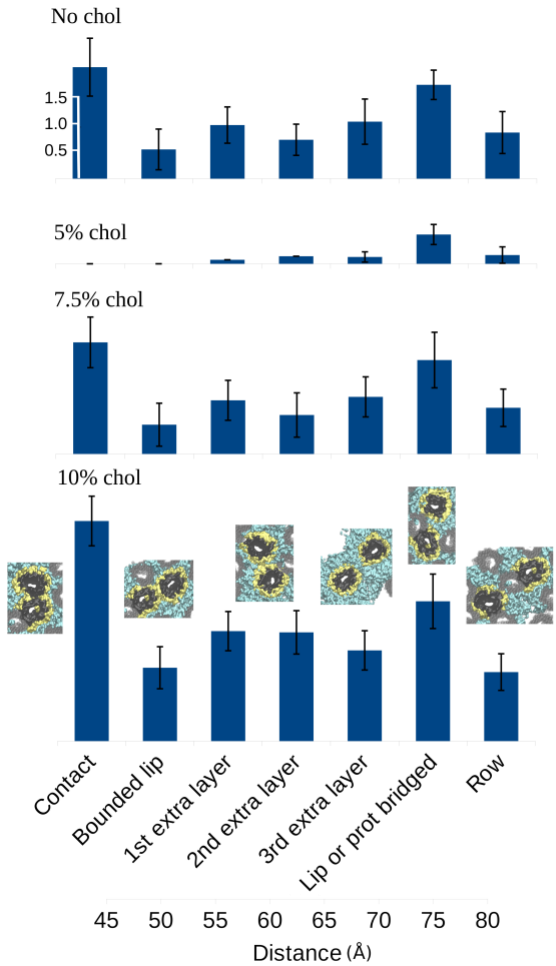

Fig. 5: Cholesterol triggers reassembly of VDAC clusters. The distance between the VDAC particles was obtained from the VDAC positions on the AFM micrographs. The following context was assigned on the basis of the computed assembly models: contact [<46 Å]; bounded lip [46-50 Å]; 1st extra layer [50-56 Å]; 2nd extra layer [56-62 Å]; 3rd extra layer [62-68 Å]; lipid or protein bridged [68-80 Å]; and row [80-86 Å]. The scale bar represents the number of occurrences (in percent) relative to all protein-protein distances observed in the various models. Error bars represent the standard deviation from multiple calculations (see Methods). Model vignettes were extracted from the molecular models corresponding to the given distance measurements. A bound lipid is a situation in which proteins are bridged by lipids assigned in MD, affecting the first lipid shell. The subsequent lipid layers correspond to the lipid shells observed in the MD simulations, illustrated in SFig. 7. At each distance, protein separation may result from a mixture of lipid- and protein-mediated interactions following local protein density.

VDAC has different affinities for MOM lipids

To understand VDAC-lipid interactions, we conducted MD simulations of monomeric VDAC1 in membranes mimicking two levels of MOM complexity: simple membrane 1 (SM1, POPC/POPE at 65/35 (w:w)) and simple membrane 2 (SM2, POPC/POPE/Chol/cardiolipin at 62.5/31.5/5.3/1.1 (w:w)). Despite initially random lipid distributions, convergence occurred across three independent MD simulations for each system on the microsecond timescale. Analysis of lipid positions over the final 10 µs revealed consistent distributions across replicates (SFig. 8). The probabilities of presence of each lipid from the simulations for SM1 (upper row) and SM2 (lower row) were averaged over 3000 frames and shown in Fig. 6.

In SM1 (Fig. 6a-c), POPE is preferentially positioned close to the protein, whereas POPC forms a ring of lipids farther away. The coarse-grained representation of lipids gives rise to a highly anisotropic distribution of both lipid types around VDAC1, despite subtle differences between the PC and PE head groups. This anisotropic distribution of lipids extended radially to the bulk, demonstrating long-range effects (at least 50 Å from the protein surface), as observed for other proteins[39]. Adding cholesterol and trace amounts of cardiolipins to SM1, we created SM2. On the timescale of our study (20 µs), the distribution of cardiolipins was meaningless and suffered from poor convergence owing to its low concentration. In contrast, the behavior of cholesterol showed strong convergence (Fig. 5d-e), challenging the role of POPE in the proximal layer, with less impact on PC densities.

In both SM1 and SM2, the upper leaflet (cytosolic side) predominantly accommodated sites for interactions between PE and cholesterol, while the inter-membrane space leaflet exhibited a preference for PC lipid concentration (Fig. 5c,f, the side view of lipid distribution is asymmetric between membrane leaflets). Notably, both leaflets contained equal numbers of lipids. We conclude that VDAC can organize the lipids around itself, with a preference for cholesterol, that the POPE lipids are in direct contact with the protein, and that the POPC is in the second layer.

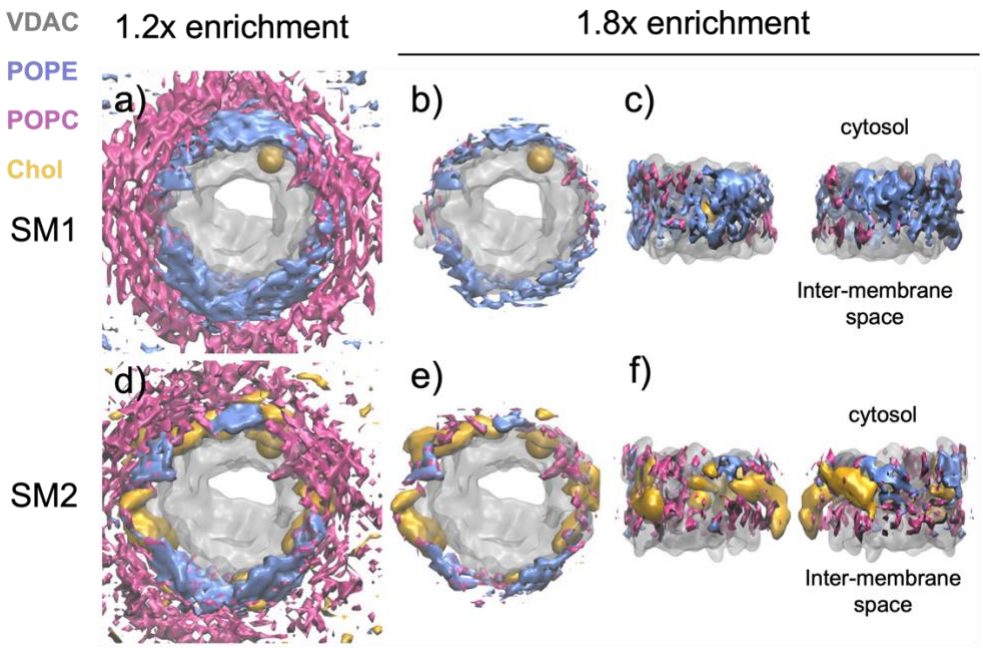

Fig. 6: VDAC organizes lipids. The displayed volumetric maps represent the individual lipid occupancies computed from molecular dynamics simulations of VDAC1. The enrichment of each lipid around VDAC is calculated relatively to the average density of each individual lipid. The upper row (**a, b, c**) show the data for the simple membrane 1 (POPC/POPE 65/35) and the lower row (**d, e, f**) is for the simple membrane 2 (POPC/POPE/Chol/CL 58/31/10/1). The mean occupancies of POPC (blue), POPE (magenta) lipids, and cholesterol (gold) were calculated over the last 10 µs of three 20 µs coarse-grained molecular dynamics simulations, the upper rows show the averaged map corresponding to the three distinct simulations of SM1. The lower row represents a similar extraction for SM2. . The top view is from the cytosol. Brown spheres indicate the position of E73, a charged amino acid, facing the membrane. The cytosolic side accommodates sites for interactions between PE and cholesterol, while the intermembrane space leaflet exhibits preference for PC lipids.

Discussion

Lipid composition and ratios govern VDAC assembly

The native MOM contains more than 30 different lipids with diverse polar heads and acyl chains. We demonstrated that within a narrow range of lipid compositions mimicking MOM with only its three main lipids, VDAC can adopt various oligomeric structures resembling those seen in native membranes[1,2], where both large, compact structures and smaller oligomers have been observed. VDAC organization observed in native MOM can only be replicated under conditions mimicking MOM composition, even with just two lipids. Consequently, we infer that VDAC organization is finely attuned to MOM lipid composition, with minor ratio changes triggering significant reorganization of VDAC assemblies.

Herein, our controlled, simplified two- or three-lipid system (POPC, POPE, and cholesterol) allowed for detailed investigation of the influence of each lipid on VDAC assembly. In membranes containing only POPC and POPE at MOM-like ratios, stable, compact assemblies resembling a “honeycomb” structure form. The addition of as little as 2% cholesterol led to more dispersed structures. We hypothesize that addition of 2% cholesterol disrupts the PE network at the protein contact, without being

able to replace it, thus triggering disorganization of the honeycomb cluster. When cholesterol content was increased, more cholesterol molecules bound around the protein and allowed the assembly of VDAC to return to a honeycomb structure, with 7.5% cholesterol content being very close to the situation without cholesterol (Fig. 5). Addition of 10% cholesterol increased even more the compaction of the VDAC structures (SFig. 5). A glass-like (i.e., amorphous and disorganized) organization[35] exists between lipids and proteins in all these assemblies, maintaining stability on the minute timescale of AFM imaging. These observations raise questions about (i) the molecular interactions driving VDAC's adaptable aggregation behavior and the stability of these assemblies, and (ii) how lipids can drive VDAC's reorganization in the membrane and its ability to form various assemblies. Both aspects are addressed in the following paragraphs.

Forces modulating membrane protein assembly

For any membrane protein, the balance between aggregation and dispersion is crucial for dynamic cellular responses, particularly signaling. VDAC experiences a hydrophobic mismatch with the membrane thickness, shown in SFig. 9, where the hydrophobic face of the protein is only 24 Å, significantly smaller than biological membranes. This mismatch acts as a long-range perturbator, generally leading to protein aggregation to minimize perturbation, similar to phase separation. In complex lipid mixtures, hydrophobic mismatches can lead to lipid sorting, particularly on the protein surface. Specific lipid binding and exchange influences protein association, especially if these interactions alleviate mismatch effects[39]. VDAC-cholesterol interactions, demonstrated experimentally[29] and in MD simulation (Fig. 6), explain VDAC's sensitivity to cholesterol concentration. The relatively small hydrophobic length of cholesterol compared with other lipids may buffer the tendency of such a short (2.4 nm) protein to aggregate, creating a physical barrier that opposes protein aggregation.

Both direct protein-protein and lipid-mediated interactions were present, varying significantly across different assemblies (models in Fig. 4 and SFig. 5), highlighting their sensitivity to lipid composition. Multiple cholesterol interaction sites on the VDAC surface make the effects of cholesterol addition on protein oligomerization complex, explaining the diversity observed by AFM. Binding site occupancy by cholesterol or other lipids influences whether aggregation or dispersion occurs, resulting in the observed balance between aggregated and lipid-separated proteins. In the interior of the highly dense honeycomb-like assemblies of VDAC proteins, we found lipid-only domains without proteins (Fig. 4l, m). We hypothesize that proteins select the optimal type and number of lipids to form specific assemblies, with leftover lipids segregating into patches.

Structural rigidity of assemblies

A common feature of all these assemblies is their stability, where lipids act as molecular "mortar" to stabilize VDAC organization in lipid-protein clusters. This lipid-mediated organization is similar to that observed in the *E. coli* outer membrane, where lipopolysaccharides primarily mediate protein-protein interactions[40]. Achieving structural rigidity with purely miscible lipids is challenging, as they do not undergo phase separation at relatively high temperatures (SFig. 1). Rigidity is achieved without cholesterol and at 10% cholesterol, with 80% of lipids within 40 Å of a protein center, in direct proximity to a protein surface. At 7.5% cholesterol, a distance of 48 Å (an additional lipid layer) is required to achieve similar rigidity. In these assemblies, most lipids are influenced by several proteins, collectively stabilizing the structural order of the mixed protein-lipid aggregates.

This scenario changes in the 5% cholesterol system, where lipids are predominantly distant from proteins, and less than 30% of lipids reside within 50 Å of any discernible protein. Lipids bridging successive proteins may be sufficiently immobilized to act akin to mortar.

VDAC preferentially binds POPE and cholesterol

MD simulations have elucidated VDAC's favored affinity for POPE and particularly cholesterol for both of which binding sites were identified on VDAC[25,29]. Affinity depends on local lipid concentration; hence, lipid ratios participate in controlling the precise lipid environment surrounding VDAC and can explain the presence of honeycombs at PE:PC (65:35) and not (50:50).

As we did not observe any glass-like structure of stable VDAC-lipid organization using only POPC and cholesterol, we conclude that our simplified three-lipid system POPE is necessary for honeycomb formation and cannot be replaced by cholesterol, even at higher concentrations. Furthermore, cholesterol exerts a significant influence on VDAC packing within the honeycomb structure, fostering larger, more compact clusters at higher concentrations (SFig. 5), whereas lower levels lead to smaller patches with reduced compaction, both assemblies previously identified in native membranes[1,2]. This suggests, as expected, that lipids are not homogeneously distributed in the native MOM, and the diversity of assemblies observed previously by AFM is probably a result of variations in the local lipid environment. We hypothesize that areas of different compactions could participate in the recruitment of certain partner proteins. PE and cholesterol have emerged as pivotal regulators of VDAC clustering.

Physiological relevance of organizations

We identified diverse organizations of VDAC, primarily characterized by a honeycomb pattern, consistent with previous findings on native membranes[1,2] and mitochondrial vesicles from *Neurospora crassa* by negative staining (Fig. 2), indicating the physiological relevance of these structures obtained in simplified membrane environments. The observed heterogeneity and lipid-rich nature of these honeycombs likely contribute to the multitude of oligomeric forms identified after detergent solubilization from native sources[41]. The diverse inter-protomer interaction areas potentially result in the dissociation of honeycomb structures and the preservation of only direct protein-protein interactions.

In MOM, VDAC exhibits a parallel organization attributed to its insertion process, whereas mVDAC1 has been observed to crystallize as antiparallel dimer in DMPC lipids[36,42]. Here, we observed parallel assemblies of mVDAC1 within honeycomb clusters (Fig. 3 and SFig. 4). We propose that the lipid asymmetry represented in our MD simulations between the leaflets (Fig 6) counterbalances protein asymmetry, thereby enabling parallel packing.

However, deviations in the lipid environment from the physiological MOM composition led to the disassembly of native VDAC structures, replaced by smaller, more dynamic, oligomers. This highlights the significant influence of the surrounding lipid composition on the stability and structural integrity of VDAC assemblies.

Lipid variations in the MOM

The sensitivity of VDAC oligomeric organization to lipid composition has significant physiological implications given the diversity in lipid composition across MOMs. Mitochondria are multifaceted, with distinct biological functions and can vary in lipid composition[43]. Furthermore, within individual mitochondria, MOM lipid composition can vary substantially owing to interactions with neighboring membranes, such as mitochondrial inner membrane (MIM)/MOM or ER/MOM contact sites, facilitating lipid transfer. Additionally, changes in MOM lipid composition occur under various physiological conditions; for instance, cancer cells exhibit altered lipid metabolism and membrane composition[31]. Furthermore, the dysregulated accumulation of cholesterol in mitochondrial membranes influences their physical properties, modulating mitochondrial permeability transition pore dynamics during cell death induction by Bax and death ligands[44,45]. In neurodegenerative conditions such as Alzheimer's disease, a change in mitochondrial lipid profiles is also observed[32], including increased mitochondrial cholesterol levels[33,46,47], which is particularly relevant given VDAC's involvement in Alzheimer pathology[48]. Therefore, our findings suggest that lipid variation could serve as an effective mechanism for regulating VDAC organization, offering flexibility, given the MOM's propensity for rapid changes in lipid composition due to lipid flux and membrane interactions.

The importance of VDAC oligomeric state in the MOM

VDAC oligomerization is implicated in crucial physiological processes, notably in apoptosis[49] and diseases such as lupus[8]. During apoptosis, VDAC oligomerization has been observed using in-cell crosslinking, resulting in a proposed model involving the formation of a mega-pore inside a ring of multiple VDAC1 molecules[49]. We could not observe this VDAC mega-pore under any of our experimental conditions. Moreover, this model contradicts thermodynamic principles because of VDAC's hydrophobic exterior, which makes it challenging to form a hydrophilic pore. We suggest that the observed VDAC clustering in our study, particularly favored by increased cholesterol, may represent VDAC oligomerization. VDAC recruits pore-forming proteins Bax and Bak, which are responsible for MOM permeability[50,51]. Therefore, such clustering could serve as a platform for the recruitment of these partners and subsequent pore formation in the MOM. Supporting this hypothesis, some models suggest that Bax and Bak bind to multimeric VDAC complexes[52].

Mitochondrion-associated membranes (MAMs), where the endoplasmic reticulum (ER) and mitochondria interact, are the central hubs for lipid and calcium transport. Lipid exchange at MAMs involves the shuttling of ER-synthesized lipids, including cholesterol, into the outer leaflet of the MOM. These lipids are then transported to the inner leaflet and subsequently to MIM. Recent findings by Jahn et al. demonstrated that VDAC acts as a lipid scramblase at the MOM but is only active in a multimeric form[9]. Based on our observations, the higher cholesterol content in MAMs[53] likely favors the formation of VDAC clusters, which could provide more efficient lipid scrambling. Furthermore, substantial calcium flux between the ER and mitochondria occurs in MAMs, mediated by the inositol trisphosphate receptor (IP3R) in the ER membrane and VDAC in the MOM[54,55]. IP3R forms large mega-Dalton tetrameric complexes, in direct contact with VDAC, as shown by co-immunoprecipitation[56]. IP3R releases large amounts of calcium into the intermembrane space, which is channeled through VDAC into the MOM via passive diffusion. To provide efficient calcium transfer, a large number of VDAC molecules are necessary (Fig. 6d illustrates the difference in size between both proteins). We propose that VDAC clustering, favored by increased cholesterol content in MAMs, facilitates efficient calcium import into the mitochondria.

Another example of VDAC clusters in the MOM is VDAC organization in sperm mitochondria. Leung et al. used cryo-electron tomography to show that an array of VDAC is used as a platform to recruit glycerol kinase, serving to tether neighboring mitochondria together[57].

VDAC was initially discovered as an ion channel, although its role has expanded with implication in various pathways. There is debate surrounding whether VDAC oligomerization affects gating and conductance. Our findings demonstrate that 10% cholesterol triggers honeycomb formation, resulting in a locally high concentration of VDACs. However, even at higher cholesterol concentrations (25%), VDAC maintains consistent conductance and gating properties[24]. We propose that a higher local flow of ions and metabolites may be achieved by increasing the density of VDAC in the membrane through honeycomb formation without altering the single-channel characteristics.

VDAC can exist in different oligomeric forms in the MOM[1,2], fulfilling different physiological functions (Fig. 7): from single-channels that conduct ions and metabolites and can recruit partner proteins such as tubulin or α-synuclein[12,14], to small oligomers like dimers that scramble lipids, and large clusters serving as a platform for protein tethering at the MOM (Fig. 7c) or efficient calcium flow (Fig. 7d). These different assemblies can be regulated by the local lipid content in the membrane, allowing the formation of different VDAC assemblies in different areas of the MOM.

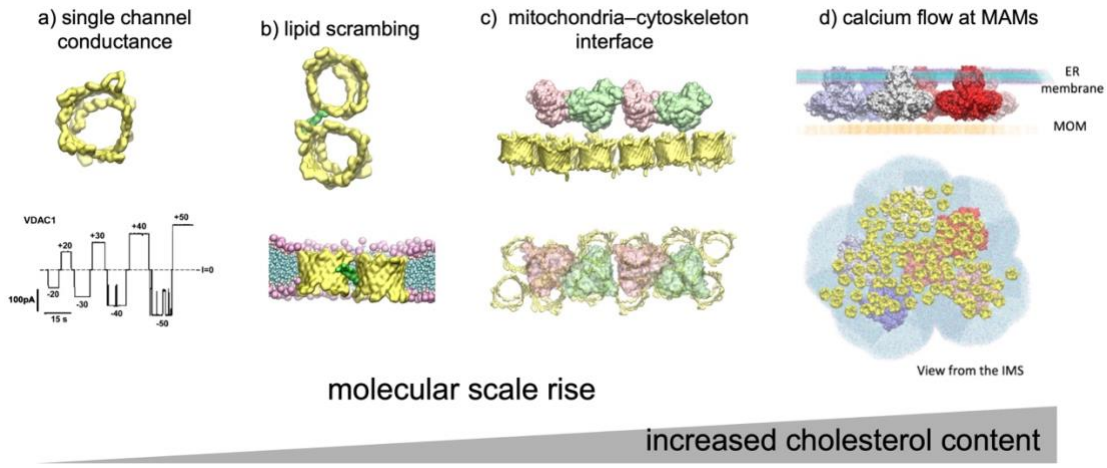

Fig 7: Lipid-induced clustering of VDAC can be associated with different biological events. a Single channel can conduct ions and metabolites. **b** Jahn et al.[9] identified a specific VDAC dimer interface involving strands β1,2 and 18-19 on the second protomer involved in lipid scrambling. In the honeycombs, we identified many protein-protein contacts that could serve to scramble lipids. **c** Arrays of VDAC serve as docking platform for glycerol kinase in sperm mitochondria (PDB ID: 7NIE).[57] **d** Model of the IP3R-VDAC complex implicated in calcium flow. Bartok et al.[56] demonstrated the presence of clusters of IP3R at ER-mitochondria contact sites, forming direct contacts with VDAC. As VDAC is thinner than the membrane, only proteins are depicted in the MOM.

Conclusion:

VDAC oligomerization and complex interaction networks are of great interest. They have implications in many major physiological processes, yet direct visualization of their organization in membranes at the molecular level remains challenging. AFM is the technique of choice for investigating membrane interactions. Expanding upon previous AFM imaging studies[1,2], our findings demonstrate that VDAC1 assembly in the membrane is profoundly influenced by lipid content, providing a mechanism for the flexible and rapid reorganization of VDAC in the MOM in response to changing conditions. Hence, VDAC can exist in various oligomeric assemblies ranging from more compact to less compact structures, which are finely tuned by the local lipid composition of the membrane. This likely serves as a regulatory mechanism for VDAC, potentially favoring local ion flows in the membrane or serving as platforms for the recruitment of specific partners to either monomeric or multimeric VDAC forms.

Methods

VDAC production and purification

The mouse VDAC1 gene bearing a 6-his tag in N-terminus inserted into the pQE9 vector was transformed into M15 *E. coli* cells for protein expression. Cells were grown at 37°C in LB medium to A_{600}= 0.8 and induced with 0,4 mM IPTG for 4 h. Cells were harvested and resuspended in 50mMTris HCl (pH 8.0), 2 mM EDTA, 20% sucrose, 0,6% Triton X-100, 0,1 mg/ml lysozyme. The resuspended pellet was sonicated and centrifuged (12,000xg, 15 min) to obtain inclusion bodies. The inclusion body pellet was washed with wash buffer [20 mM Tris HCl (pH 8.0), 300 mM NaCl, 2 mM CaCl2], repelleted and solubilized in equilibration buffer [20 mM Tris HCl (pH 8.0), 300 mM NaCl, 8 M urea]. VDAC1 was purified from solubilized inclusion bodies by Ni-NTA metal affinity column, equilibrated in equilibration buffer, washed with equilibration buffer containing 30 mM imidazole and eluted with equilibration buffer containing 150 mM imidazole. The urea-solubilized protein was concentrated to 250-300uM in an Amicon-10. 1ml of urea-solubilized protein was then rapidly diluted in 9ml of chilled 20mM tris buffer pH 8.0, 150mM NaCl, 1.5% LDAO, 5mM DTT and kept for 5-6 hours at 4°C on rotation. The 10ml protein solution was then transferred to a 7-kDa dialysis bag and dialyzed against 1L of chilled 20mM tris buffer pH 8.0, 150mM NaCl, 2mM DTT overnight at 4°C. The next day, refolded protein was collected and ultracentrifuged at 355,000g for 45 minutes to remove

aggregates. Protein was concentrated in an Amicon-50 and injected on a Superdex 200 increase 10/300 GL column equilibrated with 20mM tris buffer pH 8.0, 150mM NaCl, 0.1% LDAO, 2mM DTT. The monomeric VDAC peak was collected and concentrated to 2mg/ml. Stocks were flash frozen in liquid nitrogen and stored in 20% glycerol at -80°C. Samples were ultracentrifuged after thawing before reconstitution into liposomes to remove any possible aggregates.

Reconstitution into liposomes

POPE, POPC and cholesterol lipids were purchased from Avanti polar lipids in chloroform, mixed at the desired ratios and dried under nitrogen gas. The resulting lipid film was resuspended by vortexing in 150mM KCl, 20 mM Tris pH8 to a final concentration of 12,5 mg/ml of lipids. The suspension was heated at 37°C for 10 min then sonicated for 1 min or until formation of small unilamellar vesicles (100nm), as measured by dynamic light scattering (DLS). Detergent β-OG was added to a 0.65 detergent/lipid ratio (w:w). Proteins were added to the destabilized liposomes to a 3:1 lipid:VDAC ratio (w:w). Detergent removal was achieved by addition of Bio-beads at a Bio-bead/detergent ratio of 30 (w:w) overnight. The liposomes were analyzed by DLS after reconstitution.

AFM and HS-AFM data acquisition

To form a homogeneous protein containing supported lipid bilayer (SLB), a mixture of 15 µl of the proteoliposome suspension (1 mg/ml) and 85 µl of "Incubation buffer" (10 mM HEPES pH 7.4, 100 mM NaCl, 15 mM CaCl2) was incubated 1h at room temperature on a freshly cleaved mica under a humid hood. The sample was rinsed 10 times in ultrapure water (MilliQ) and imaged by AFM/HS-AFM in "Imaging buffer" (10 mM HEPES pH 7.4, 100 mM NaCl, 5 mM CaCl2) at 35 °C to check the homogeneity of the formed membrane. All conditions have been performed in triplicates.
Conventional AFM imaging was performed in contact mode with a Nanoscope IIIe Multimode AFM (Bruker, Santa Barbara, CA, USA) using OTR4 probes of k=0.1 N/m. The scan rate, gains and deflection setpoint were adjusted during acquisition to optimise the quality of acquired images.
HS-AFM movies were acquired in amplitude modulation mode optimised high–resolution imaging parameters with a modified HS-AFM (SS-NEX, RIBM, Tsukuba, Japan)[58]. The apparatus is equipped with our custom-made digital high-speed lock-in amplifier coded on a reconfigurable FPGA using LabView (National Instruments, Austin, USA). Short cantilevers (length ~7 µm) designed for HS–AFM, presenting an electron beam deposition (EBD) tip, were used (USC-F1.2-k0.15 Nanoword, Switzerland). They are characterised by a nominal spring constant k = 0.15 N/m, a resonance frequency in liquid of fres = 500 kHz and a quality factor Qc ~ 2 (in liquid). HS-AFM sensitivity to probe the deflection was 0.1 V/nm. The imaging amplitude setpoint was set to ~90% of the free amplitude (~10 Å). All experiments were performed at 35°C, by introducing the HS-AFM microscope inside a temperature-controlled box.

Image analysis

Acquired images were plane-fit and flattened using the AFM processing and analysis software provided by the instrument manufacturer. HS AFM image treatment was limited to the correction of XY drift and a first order X-line fit. Image analysis was performed using the general distribution of ImageJ[59] and of WSxM[60].
To study the particle distribution, the computation of the radial distribution function was implemented. This measure is obtained by computing the particle density in a ring of radius *r* and thickness *dr* for each particles and then averaging. To exclude, or not, the heterogeneity effect due to the border, particularly in small patches, a code has been developed (Python, scipy and shapely packages). It computes the enclosing region by determining the concave surface which include all the particles. Next, to correct the radial distribution, the density computation uses the intersection surface between the ring and the enclosing surface. The radial distribution function (RDF) was also used as the primary data to compute the normalized distribution of protein-protein distances shown in Fig. 5; where the error bars represent

the standard deviation from multiple calculations of the distribution (100, except for 89 in the smallest cluster). Each individual calculation was built using all proteins within a 200 Å radius around each randomly selected protein, and making the distance statistic from 0 to 100 Å. Averages and standard deviations across the multiple calculations were used to construct the histograms.

Coarse grain setup and molecular dynamics simulations

The coarse grain structure of hVDAC1 was based on that of mouse VDAC1 (PDB ID: 3EMN)[42] that contain only 4 conservative mutations over 254 residues. First the homology modeling was set up using MODELLER[61]. Then the protein was embedded in membranes using the CG membrane builder[62] tool from CHARM-GUI[63] using the MARTINI 2.2 force field[64] with elastic networks[65]. Two distinct membrane were build based on the main lipids of the MOM membrane[34] (Table S1). The first one (SM1) is made only of POPC and POPE (65:35 mol:mol, 64:36 w:w) and the second one (SM2) contain 10 % molar cholesterol. The final systems comprise 1100 lipids, that were randomly distributed in periodic rectangular boxes, that also contains 13000 CG water particles and 100 mM NaCl. Three distinct systems were built for each membranes. The various systems, were heated (to 323 K), equilibrated and run over 20 µs using the default protocol and parameters provided by Charmm-GUI. The simulation were run on the supercomputer facilities provided by the GENCI at the CINES - Montpellier – France- or at the TGCC (CEA) – Saclay France using Gromacs v2018[66].

Building of model assemblies

The coordinates extracted from the AFM micrographs, were used to position proteins and lipids extracted from MD configurations of the monomeric systems. Distinct configurations were randomly chosen from the last 10 µs of the various MD simulations. The proteins were extracted with a cylindrical extrusion of lipids with a radius of 50 Å about the protein center. Since the experimental orientation of the individual proteins is unknown, we randomly rotated the proteins and their associated lipids around the channel axis, which is perpendicular to the membrane plane. An optimization procedure was developed to select orientations that minimize clashes between proteins. In this python program, overlapping lipids from the added configurations were sequentially removed from the model. The resulting stereochemical models were used to evaluate lipid-protein and inter-protein contacts in order to gain insights into the assemblies at the molecular level.

Screening of outer membrane vesicles by negative staining microscopy

Outer membrane vesicles (OMVs) isolated from *Neurospora crassa* mitochondria were kindly provided by Prof. Stephan Nussberger (see [67]). Frozen OMVs were thawed and applied onto copper grids (400 mesh) backed with a continuous carbon layer, and subsequently stained with uranyl formate. Data was collected using a Tecnai Spirit Biotwin electron microscope at 120 kV (FEI), fitted with a CCD camera (Gatan). Micrographs were acquired with 2 s exposure at 49,000x, 68,000x and 76,000x nominal magnification.

Acknowledgements
This work was supported by the Aix-Marseille Université grant AMX-21-PEP-022 (L.B.), PhD fellowships from Aix-Marseille Université (E.L. and V.R.) and French grants ANR-21-CE42-0031 and ANR-19-CE11-0024 (I.C.). This work was performed using HPC resources from GENCI–IDRIS (Grant 2020-A0080707044, and 2021-A0110707044). Mitochondria and ER in Fig. 6 are from Servier Medical Art. Servier Medical Art by Servieris licensed under a Creative Commons Attribution 3.0. Unported License (https://creativecommons.org/licenses/by/3. 0/)

Author contributions
Conception: LB, JPD, IC. Sample preparation: LB, VR ; AFM imaging: EL, NB ; Computational and molecular modeling: JPD ; Data analysis: JPD, EL, AO, JS, IC, NB, LB ; Negative stain : PO. LB and JPD wrote the manuscript. All the authors reviewed it.

Competing interests
We declare no competing interests.

References:

1. Gonçalves, R. P., Buzhynskyy, N., Prima, V., Sturgis, J. N. & Scheuring, S. Supramolecular assembly of VDAC in native mitochondrial outer membranes. *J. Mol. Biol.* **369**, 413–418 (2007).
2. Hoogenboom, B. W., Suda, K., Engel, A. & Fotiadis, D. The supramolecular assemblies of voltage-dependent anion channels in the native membrane. *J. Mol. Biol.* **370**, 246–255 (2007).
3. Chin, H. S. *et al.* VDAC2 enables BAX to mediate apoptosis and limit tumor development. *Nat. Commun.* **9**, 4976 (2018).
4. Roy, S. S., Ehrlich, A. M., Craigen, W. J. & Hajnóczky, G. VDAC2 is required for truncated BID-induced mitochondrial apoptosis by recruiting BAK to the mitochondria. *EMBO Rep.* **10**, 1341–1347 (2009).
5. van Delft, M. F. *et al.* A small molecule interacts with VDAC2 to block mouse BAK-driven apoptosis. *Nat. Chem. Biol.* **15**, 1057–1066 (2019).
6. Sander, P., Gudermann, T. & Schredelseker, J. A Calcium Guard in the Outer Membrane: Is VDAC a Regulated Gatekeeper of Mitochondrial Calcium Uptake? *Int. J. Mol. Sci.* **22**, 946 (2021).
7. Shankar, T. S. *et al.* Cardiac-specific deletion of voltage dependent anion channel 2 leads to dilated cardiomyopathy by altering calcium homeostasis. *Nat. Commun.* **12**, 4583 (2021).
8. Kim, J. *et al.* VDAC oligomers form mitochondrial pores to release mtDNA fragments and promote lupus-like disease. *Science* **366**, 1531–1536 (2019).
9. Jahn, H. *et al.* Phospholipids are imported into mitochondria by VDAC, a dimeric beta barrel scramblase. *Nat. Commun.* **14**, 8115 (2023).
10. Shoshan-Barmatz, V., Maldonado, E. N. & Krelin, Y. VDAC1 at the crossroads of cell metabolism, apoptosis and cell stress. *Cell Stress* **1**, 11–36 (2017).
11. Yuan, Z. *et al.* Key residues in the VDAC2-BAK complex can be targeted to modulate apoptosis. *PLOS Biol.* **22**, e3002617 (2024).
12. Rostovtseva, T. K. *et al.* Tubulin binding blocks mitochondrial voltage-dependent anion channel and regulates respiration. *Proc. Natl. Acad. Sci. U. S. A.* **105**, 18746–18751 (2008).
13. Rovini, A. Tubulin-VDAC Interaction: Molecular Basis for Mitochondrial Dysfunction in Chemotherapy-Induced Peripheral Neuropathy. *Front. Physiol.* **10**, 671 (2019).
14. Jacobs, D. *et al.* Probing Membrane Association of α-Synuclein Domains with VDAC Nanopore Reveals Unexpected Binding Pattern. *Sci. Rep.* **9**, 4580 (2019).
15. Queralt-Martín, M. *et al.* A lower affinity to cytosolic proteins reveals VDAC3 isoform-specific role in mitochondrial biology. *J. Gen. Physiol.* **152**, (2020).
16. Shoshan-Barmatz, V., Pittala, S. & Mizrachi, D. VDAC1 and the TSPO: Expression,

Interactions, and Associated Functions in Health and Disease States. *Int. J. Mol. Sci.* **20**, 3348 (2019).
17. Pastorino, J. G. & Hoek, J. B. Regulation of hexokinase binding to VDAC. *J. Bioenerg. Biomembr.* **40**, 171–182 (2008).
18. Dolder, M. *et al.* Crystallization of the human, mitochondrial voltage-dependent anion-selective channel in the presence of phospholipids. *J. Struct. Biol.* **127**, 64–71 (1999).
19. Betaneli, V., Petrov, E. P. & Schwille, P. The role of lipids in VDAC oligomerization. *Biophys. J.* **102**, 523–531 (2012).
20. Bayrhuber, M. *et al.* Structure of the human voltage-dependent anion channel. *Proc. Natl. Acad. Sci.* **105**, 15370–15375 (2008).
21. Bergdoll, L. A. *et al.* Protonation state of glutamate 73 regulates the formation of a specific dimeric association of mVDAC1. *Proc. Natl. Acad. Sci. U. S. A.* **115**, E172–E179 (2018).
22. Schredelseker, J. *et al.* High resolution structure and double electron-electron resonance of the zebrafish voltage-dependent anion channel 2 reveal an oligomeric population. *J. Biol. Chem.* **289**, 12566–12577 (2014).
23. Rostovtseva, T. K., Kazemi, N., Weinrich, M. & Bezrukov, S. M. Voltage gating of VDAC is regulated by nonlamellar lipids of mitochondrial membranes. *J. Biol. Chem.* **281**, 37496–37506 (2006).
24. Queralt-Martín, M. *et al.* Assessing the role of residue E73 and lipid headgroup charge in VDAC1 voltage gating. *Biochim. Biophys. Acta Bioenerg.* **1860**, 22–29 (2019).
25. Mlayeh, L., Krammer, E.-M., Léonetti, M., Prévost, M. & Homblé, F. The mitochondrial VDAC of bean seeds recruits phosphatidylethanolamine lipids for its proper functioning. *Biochim. Biophys. Acta Bioenerg.* **1858**, 786–794 (2017).
26. Rostovtseva, T. K., Gurnev, P. A., Chen, M.-Y. & Bezrukov, S. M. Membrane lipid composition regulates tubulin interaction with mitochondrial voltage-dependent anion channel. *J. Biol. Chem.* **287**, 29589–29598 (2012).
27. Budelier, M. M. *et al.* Photoaffinity labeling with cholesterol analogues precisely maps a cholesterol-binding site in voltage-dependent anion channel-1. *J. Biol. Chem.* **292**, 9294–9304 (2017).
28. Budelier, M. M. *et al.* Click Chemistry Reagent for Identification of Sites of Covalent Ligand Incorporation in Integral Membrane Proteins. *Anal. Chem.* **89**, 2636–2644 (2017).
29. Cheng, W. W. L. *et al.* Multiple neurosteroid and cholesterol binding sites in voltage-dependent anion channel-1 determined by photo-affinity labeling. *Biochim. Biophys. Acta Mol. Cell Biol. Lipids* **1864**, 1269–1279 (2019).
30. Hosaka, T. *et al.* Crystal structural characterization reveals novel oligomeric interactions of human voltage-dependent anion channel 1. *Protein Sci. Publ. Protein Soc.* **26**, 1749–1758 (2017).
31. Poulaki, A. & Giannouli, S. Mitochondrial Lipids: From Membrane Organization to Apoptotic Facilitation. *Int. J. Mol. Sci.* **23**, 3738 (2022).
32. Kurokin, I. *et al.* Targeted Lipidomics of Mitochondria in a Cellular Alzheimer's Disease Model. *Biomedicines* **9**, 1062 (2021).
33. Fernández, A., Llacuna, L., Fernández-Checa, J. C. & Colell, A. Mitochondrial cholesterol loading exacerbates amyloid beta peptide-induced inflammation and neurotoxicity. *J. Neurosci. Off. J. Soc. Neurosci.* **29**, 6394–6405 (2009).
34. Horvath, S. E. & Daum, G. Lipids of mitochondria. *Prog. Lipid Res.* **52**, 590–614 (2013).
35. Munguira, I. *et al.* Glasslike Membrane Protein Diffusion in a Crowded Membrane. *ACS Nano* **10**, 2584–2590 (2016).
36. Ujwal, R., Cascio, D., Chaptal, V., Ping, P. & Abramson, J. Crystal packing analysis

of murine VDAC1 crystals in a lipidic environment reveals novel insights on oligomerization and orientation. *Channels Austin Tex* **3**, 167–170 (2009).
37. Ardail, D. *et al.* Mitochondrial contact sites. Lipid composition and dynamics. *J. Biol. Chem.* **265**, 18797–18802 (1990).
38. Ferreira, T. M. *et al.* Cholesterol and POPC segmental order parameters in lipid membranes: solid state 1H–13C NMR and MD simulation studies. *Phys. Chem. Chem. Phys.* **15**, 1976–1989 (2013).
39. Duneau, J.-P., Khao, J. & Sturgis, J. N. Lipid perturbation by membrane proteins and the lipophobic effect. *Biochim. Biophys. Acta Biomembr.* **1859**, 126–134 (2017).
40. Webby, M. N. *et al.* Lipids mediate supramolecular outer membrane protein assembly in bacteria. *Sci. Adv.* **8**, eadc9566 (2022).
41. Zalk, R., Israelson, A., Garty, E. S., Azoulay-Zohar, H. & Shoshan-Barmatz, V. Oligomeric states of the voltage-dependent anion channel and cytochrome c release from mitochondria. *Biochem. J.* **386**, 73–83 (2005).
42. Ujwal, R. *et al.* The crystal structure of mouse VDAC1 at 2.3 A resolution reveals mechanistic insights into metabolite gating. *Proc. Natl. Acad. Sci. U. S. A.* **105**, 17742–17747 (2008).
43. Monzel, A. S., Enríquez, J. A. & Picard, M. Multifaceted mitochondria: moving mitochondrial science beyond function and dysfunction. *Nat. Metab.* **5**, 546–562 (2023).
44. Montero, J. *et al.* Cholesterol and peroxidized cardiolipin in mitochondrial membrane properties, permeabilization and cell death. *Biochim. Biophys. Acta BBA - Bioenerg.* **1797**, 1217–1224 (2010).
45. Montero, J. *et al.* Mitochondrial cholesterol contributes to chemotherapy resistance in hepatocellular carcinoma. *Cancer Res.* **68**, 5246–5256 (2008).
46. Colell, A., Fernández, A. & Fernández-Checa, J. C. Mitochondria, cholesterol and amyloid beta peptide: a dangerous trio in Alzheimer disease. *J. Bioenerg. Biomembr.* **41**, 417–423 (2009).
47. Barbero-Camps, E. *et al.* Endoplasmic reticulum stress mediates amyloid β neurotoxicity via mitochondrial cholesterol trafficking. *Am. J. Pathol.* **184**, 2066–2081 (2014).
48. Magri, A. & Messina, A. Interactions of VDAC with Proteins Involved in Neurodegenerative Aggregation: An Opportunity for Advancement on Therapeutic Molecules. *Curr. Med. Chem.* **24**, 4470–4487 (2017).
49. Keinan, N., Tyomkin, D. & Shoshan-Barmatz, V. Oligomerization of the mitochondrial protein voltage-dependent anion channel is coupled to the induction of apoptosis. *Mol. Cell. Biol.* **30**, 5698–5709 (2010).
50. Ma, S. B. *et al.* Bax targets mitochondria by distinct mechanisms before or during apoptotic cell death: a requirement for VDAC2 or Bak for efficient Bax apoptotic function. *Cell Death Differ.* **21**, 1925–1935 (2014).
51. Lauterwasser, J. *et al.* The porin VDAC2 is the mitochondrial platform for Bax retrotranslocation. *Sci. Rep.* **6**, 32994 (2016).
52. Dadsena, S., Hassan, D. G. & Holthuis, J. C. M. Unraveling the molecular principles by which ceramides commit cells to death. *Cell Stress* **3**, 280–283 (2019).
53. Fujimoto, M., Hayashi, T. & Su, T.-P. The role of cholesterol in the association of endoplasmic reticulum membranes with mitochondria. *Biochem. Biophys. Res. Commun.* **417**, 635–639 (2012).
54. De Stefani, D. & Rizzuto, R. Molecular control of mitochondrial calcium uptake. *Biochem. Biophys. Res. Commun.* **449**, 373–376 (2014).
55. De Stefani, D. *et al.* VDAC1 selectively transfers apoptotic Ca2+ signals to mitochondria. *Cell Death Differ.* **19**, 267–273 (2012).

56. Bartok, A. *et al.* IP3 receptor isoforms differently regulate ER-mitochondrial contacts and local calcium transfer. *Nat. Commun.* **10**, 3726 (2019).
57. Leung, M. R. *et al.* In-cell structures of conserved supramolecular protein arrays at the mitochondria–cytoskeleton interface in mammalian sperm. *Proc. Natl. Acad. Sci.* **118**, e2110996118 (2021).
58. Ando, T. *et al.* A high-speed atomic force microscope for studying biological macromolecules. *Proc. Natl. Acad. Sci. U. S. A.* **98**, 12468–12472 (2001).
59. Schneider, C. A., Rasband, W. S. & Eliceiri, K. W. NIH Image to ImageJ: 25 years of image analysis. *Nat. Methods* **9**, 671–675 (2012).
60. Horcas, I. *et al.* WSXM: a software for scanning probe microscopy and a tool for nanotechnology. *Rev. Sci. Instrum.* **78**, 013705 (2007).
61. Webb, B. & Sali, A. Comparative Protein Structure Modeling Using MODELLER. *Curr. Protoc. Bioinforma.* **54**, 5.6.1-5.6.37 (2016).
62. Wu, E. L. *et al.* CHARMM-GUI Membrane Builder toward realistic biological membrane simulations. *J. Comput. Chem.* **35**, 1997–2004 (2014).
63. Jo, S., Kim, T., Iyer, V. G. & Im, W. CHARMM-GUI: A web-based graphical user interface for CHARMM. *J. Comput. Chem.* **29**, 1859–1865 (2008).
64. de Jong, D. H. *et al.* Improved Parameters for the Martini Coarse-Grained Protein Force Field. *J. Chem. Theory Comput.* **9**, 687–697 (2013).
65. Periole, X., Cavalli, M., Marrink, S.-J. & Ceruso, M. A. Combining an Elastic Network With a Coarse-Grained Molecular Force Field: Structure, Dynamics, and Intermolecular Recognition. *J. Chem. Theory Comput.* **5**, 2531–2543 (2009).
66. Abraham, M. J. *et al.* GROMACS: High performance molecular simulations through multi-level parallelism from laptops to supercomputers. *SoftwareX* **1**, 19–25 (2015).
67. Ornelas, P. *et al.* Two conformations of the Tom20 preprotein receptor in the TOM holo complex. *Proc. Natl. Acad. Sci. U. S. A.* **120**, e2301447120 (2023).